Journal of the European Ceramic Society **18** (1998) 1079–1087

PII: S0955-2219(98)00014-4
0955-2219/98/$19.00 + 0.00

Characterisation of Zirconia–Titania Powders Prepared by Coprecipitation

Marco Daturi, Alberto Cremona, Fabio Milella, Guido Busca and Edoardo Vogna

Istituto di Chimica, Facoltà di Ingegneria, Università di Genova, P.le Kennedy, I-16129 Genova, Italy

(Received 13 August 1997; accepted 19 December 1997)

Abstract

High surface area ZrO_2–TiO_2 powders in the entire compositional range have been prepared by a coprecipitation method. The sample with 1:1 ZrO_2:TiO_2 molar ratio is amorphous until crystallisation of $ZrTiO_4$, occurring at 970 K in DTA experiments. The presence of ZrO_2 hinders the anatase crystallisation and its transformation into rutile, while the presence of TiO_2 hinders the crystallisation of zirconia but favours monoclinic with respect to tetragonal zirconia. Solubilities of TiO_2 into the monoclinic ZrO_2 phase and into the $ZrTiO_4$ phase, as well as of ZrO_2 into the rutile phase have been found. © *1998 Elsevier Science Limited. All rights reserved*

1 Introduction

Titania powders are largely used in the pigment and catalyst industries.[1] In particular, they are widely used as heterogeneous catalysts for the selective oxidation of ortho-xylene to phthalic anhydride[2,3] and for the selective catalytic reduction of NOx by ammonia in waste gases from power stations (SCR process[4,5]). In both cases the catalysts are constituted by the anatase polymorph of TiO_2 as the support on the surface of which vanadium oxide is spread. However, these catalysts differ for the surface area of the anatase support (low for oxidation, higher for SCR), for the amount of vanadium oxide loaded and for the addition of stabilisers and/or promoters, whose role is, in most cases, not fully clear.

TiO_2-anatase has also been reported to act as an optimal support for W- and Mo-sulphide based catalysts for hydrotreatments of oil fractions.[6,7] For these applications, TiO_2-anatase is much better than alumina or silica, other typical oxide carriers.

On the other hand, deep limitations of anatase as a catalyst support are related to its sintering at relatively low temperature[8,9] and to the fact that it is a metastable phase, and tends to transform into the thermodynamically stable TiO_2 polymorph, rutile, at any temperature.[9,10] The anatase-to-rutile phase transformation can occur, in the case of highly dispersed powders, at so low temperatures as 500–600°C,[9] and the occurrence of this transition in the hot-spots of the reactor is considered to represent a main factor in catalyst deactivation in the case of the selective oxidation catalysis.[3] This has been related both to the strong decrease of the catalyst surface area upon this phase transformation, and to the intrinsically lower activity of rutile-based catalysts. On the other hand it has been reported by several authors that vanadium has a catalytic effect on the anatase sintering and on its phase transformation to rutile[9] while additives such as WO_3,[11] MoO_3[12] and K_2SO_4,[9] added to TiO_2-anatase, retard these phenomena.

Zirconia ZrO_2 can be prepared successfully in a highly dispersed form and can also act as a very good carrier for vanadia[2,3,13] and Mo or W sulphide catalysts.[5,14] Zirconia presents three polymorphic phases that are thermodynamically stable in three different temperature ranges.[10,15] The low temperature form, monoclinic ZrO_2 or baddeleyite, can reversibly transform into a tetragonal phase near 1100°C, that can convert into a cubic phase near 2400°C. However, the presence of impurity cations, such as Y^{3+}, Mg^{2+} or Ca^{2+} can stabilise the tetragonal and cubic phases down to room temperature.[16]

Due to the usefulness and limitations of TiO_2 and ZrO_2 in the catalysis field, it seemed interesting to prepare TiO_2–ZrO_2 mixed oxides and to study their structural and morphological behaviour. Similar materials are also of interest in the field of the preparation of Zr-titanate based ceramics as dielectric materials for capacitors[17] and resonator components in filters and frequency-stable oscillators.[18]

2 Experimental

Samples of the solid solution $Zr_{1-x}Ti_xO_2$ (with $x = 0$, 0·05, 0·10, 0·25, 0·50, 0·75, 0·90, 0·95, 1) have been prepared mixing carefully $Zr(NO_3)_4$ (MEL Chemicals, solution 40%) and $Ti[OCH(CH_3)_2]_4$ (Aldrich, 97%) hydrolising with water, then drying the gel at 393 K for several hours.

Nitrates and residual organic compounds have been decomposed, in air, in an electronically controlled furnace at 723 K for 4 h. The heating and cooling rate before and upon calcination was 40 K min^{-1}.

Other calcination processes up to 1273 K have been carried out in an electronically controlled furnace in which the heating and cooling rate was 10 K min^{-1}.

The XRD spectra have been recorded on a Philips PW 1710 diffractometer (Cu K_α radiation, Ni filter; 435 kV, 35 mA). Cell parameters have been calculated by a dedicated least squares software. The crystal size was evaluated by using the Scherrer's formula.[19]

The FT–IR spectra have been recorded using a Nicolet Magna 750 Fourier Transform instruments. For the region 4000–350 cm^{-1} a KBr beam splitter has been used with a DTGS detector. For the FIR region (600–50 cm^{-1}) a 'solid substrate' beam splitter and a DTGS polyethylene detector have been used. KBr pressed disks (IR region) or polyethylene pressed disks and samples deposed on Si disks (FIR region) were used.

The Ft–Raman spectra have been recorded using a Brucker Instrument. The BET surface areas have been measured by a Fisons Sorptomatic instrument by nitrogen adsorption at liquid nitrogen temperature. DTA-TG experiments were performed in air, with a Setaram TGA 92-12 apparatus, from room temperature to 1273 K, with heating and cooling rate of 10 K min^{-1}.

3 Results and Discussion

3.1 XRD and DTA characterisation

As reported in Table 1, X-ray diffraction shows that the samples with $0 \leq x \leq 0{\cdot}5$ are substantially amorphous after drying. DTA analyses of Zr-rich samples ($0 \leq x \leq 0{\cdot}1$, Fig. 1) present a broad exothermic peak in the range 673–723 K. This peak is markedly split for the sample with $x = 0{\cdot}1$. The DTA curve of the sample with $x = 0{\cdot}25$ shows an analogous split peak, but clearly shifted to higher temperatures: 890, 930 K. The DTA curve of the sample with $x = 0{\cdot}5$ shows a very intense and sharp split peak centred at 971, 975 K.

The XRD patterns of the powders with $0 \leq x \leq 0{\cdot}25$ after calcination at 723 K (Fig. 2), show a mixture of two zirconia phases: the tetragonal, space group $P4_2/nmc$, no. 137, $Z = 4$ (ICDD no. 42-1164) and the monoclinic one, S.G. $P2_1/a$, no. 14, $Z = 4$ (ICDD no. 37-1484). However, the crystallinity of such phases definitely decreases by increasing x, the sample with $x = 0{\cdot}5$ being still amorphous after this thermal treatment.

The XRD patterns of the powders with $0 \leq x \leq 0{\cdot}5$ after calcination at 1273 K are reported in Fig. 3. A large predominance of the monoclinic phase is shown for pure zirconia, although small amounts of the tetragonal phase are still present. This agrees with the thermodynamical stability of the monoclinic phase below 1373 K,[10,15] the tetragonal phase being metastable in this range.

The XRD pattern of the sample with $x = 0{\cdot}5$ after calcination at 1273 K agrees completely with that of the orthorhombic compound $ZrTiO_4$ (S.G. Pnab, no. 60, $Z = 2$, ICDD no. 34-0415). Unfortunately, most of the peaks of this compound are superimposed to peaks of monoclinic or tetragonal ZrO_2 so that it is not easy to distinguish the presence of such phase in the samples with $x < 0{\cdot}5$. Actually, the patterns for $x = 0{\cdot}05$ and 0·1 seem to be again due to a superimposition of the patterns of the two zirconia phases, with a slight increase of the tetragonal phase content by increasing x from 0 to 0·1, in agreement with the largest solubility of TiO_2 in the tetragonal phase.[20] The a and b unit cell parameters of the monoclinic phase are definitely compressed by increasing x from 0 to 0·1, while the c parameter is not. Also the unit cell parameters of the tetragonal zirconia phase are definitely contracted with respect to those reported in the literature and to those measured for this phase in samples with lower or no titanium content. This indicates that Ti enters both the monoclinic and tetragonal ZrO_2 phase in a substitutional solid solution.

These data show that pure zirconia behaves in the following way:

amorphous —700 K ⟶ monoclinic + tetragonal ⟶ monoclinic

This can occur because the higher treatment is still lower of the temperature for the thermodynamically driven monoclinic to tetragonal phase transition.[10,15] By addition of titanium the crystallisation of the ZrO_2 phase is shifted slightly upwards and the tetragonal ZrO_2 versus monoclinic ZrO_2 ratio increases at any temperature. When the $x = 0{\cdot}5$ the $ZrTiO_4$ phase is formed. In this case, however, the crystallisation temperature is definitely shifted upwards.

Table 1. XRD data on $Zr_{1-x}Ti_xO_2$ samples

Sample	*T calc. (K)*	*XRD phase*	*Cell parameters (Å)*			
			a	*b*	*c*	β
ZrO_2	623	Amorphous	—	—	—	—
	723	Tetragonal	5·112 (7)	—	5·200 (15)	—
		Monoclinic	5·298 (8)	5·219 (11)	5·153 (4)	98·71 (0·06)
	1273	Monoclinic	5·317 (4)	5·213 (3)	5·158 (3)	99·19 (0·02)
		Tetragonal	5·126 (10)	—	5·306 (9)	—
$Zr_{0.95}Ti_{0.05}$	393	Amorphous	—	—	—	—
	723	Tetragonal	5·097 (2)	—	5·174 (9)	—
		Monoclinic	5·313 (9)	5·248 (7)	5·152 (5)	99·16 (0·05)
	1273	Monoclinic	5·297 (5)	5·220 (4)	5·145 (4)	99·23 (0·02)
		Tetragonal	5·082 (9)	—	5·298 (12)	—
$zR_{0.90}Ti_{0.10}$	393	Amorphous	—	—	—	—
	723	Tetragonal	5·074 (2)	—	5·191 (5)	—
		Monoclinic	5·320 (10)	5·220 (7)	5·135 (6)	99·09 (0·05)
	1273	Monoclinic	5·278 (8)	5·206 (6)	5·097 (7)	99·03 (0·05)
		Tetragonal	5·052 (14)	—	5·257 (12)	—
$Zr_{0.75}Ti_{0.25}$	393	Amorphous	—	—	—	—
	723	Tetragonal	5·105 (6)	—	5·142 (17)	—
		Monoclinic	5·291 (4)	5·177 (6)	5·178 (14)	98·57 (0·07)
	1273	Tetragonal	5·057 (1)	—	5·218 (3)	—
		Monoclinic	5·294 (6)	5·213 (4)	5·125 (4)	98·77 (0·03)
$Zr_{0.50}Ti_{0.50}$	393	Amorphous	—	—	—	—
	723	Amorphous	—	—	—	—
	1273	$ZrTiO_4$	5·021 (5)	5·454 (4)	4·844 (5)	—
$Zr_{0.25}Ti_{0.75}$	393	Anatase	3·800 (3)	—	9·554 (11)	—
	723	Anatase	3·806 (3)	—	9·621 (17)	—
	1273	Rutile	4·619 (1)	—	2·986 (3)	—
		$ZrTiO_4$	5·008 (5)	5·491 (6)	4·774 (8)	—
$Zr_{0.10}Ti_{0.90}$	393	Anatase	3·790 (2)	—	9·466 (9)	—
	723	Anatase	3·803 (3)	—	9·569 (15)	—
		Brookite traces	—	—	—	—
	1273	Rutile	4·623 (1)	—	2·987 (1)	—
		$ZrTiO_4$ traces	—	—	—	—
$Zr_{0.05}Ti_{0.95}$	393	Anatase	3·781 (2)	—	9·427 (8)	—
	723	Anatase	3·776 (3)	—	9·526 (12)	—
		Brookite traces	—	—	—	—
	1273	Rutile	4·591 (2)	—	2·968 (2)	—
		$ZrTiO_4$ traces	—	—	—	—
TiO_2	393	Anatase	3·781 (4)	—	9·413 (11)	—
	723	Anatase	3·784 (2)	—	9·454 (6)	—
		Brookite traces	—	—	—	—
	1273	Rutile	4·592 (2)		2·959 (0)	

The XRD patterns of the Ti-rich samples ($0{\cdot}75 \leq x \leq 1$) show broad features of poorly crystalline anatase phase (S.G. $I4_1/amd$ no. 141, $Z = 4$, ICDD no. 21-1272) with small amounts of brookite (S. G. Pbca, no. 61, ICDD no. 29-1360) already after calcination at 393 K. The same phases are also present after calcination at 723 K (Fig. 4) although their crystallinity definitely decreases by increasing Zr content (decreasing x). After calcination at 1273 K (Fig. 5) the samples with $x \geq 0{\cdot}95$ only present sharp peaks of rutile phase (S. G. $P4_2/mnm$, no. 136, $Z = 2$, ICDD no. 34-0180) while the samples with $x = 0{\cdot}90$ and 0·75 are clearly constituted by a mixture of TiO_2-rutile and $ZrTiO_4$. The unit cell parameters of rutile are, however, clearly expanded by addition of Zr, in agreement with a previous work[21] while those of $ZrTiO_4$ are contracted. This shows that partial mutual solid solutions of the two phases are obtained.

DTA analyses of the pure TiO_2 sample show the exothermic peak due to anatase-to-rutile phase transition at 1050 K, while this peak seems to be broadened and shifted upwards upon Zr addition. For the sample with $x = 0{\cdot}75$ a split exothermic peak is found at 990–1015 K showing that excess of Ti hinders the crystallisation of $ZrTiO_4$.

3.2 Surface areas

The trend of the surface areas measured for the samples calcined at 723 K is shown in Fig. 6. It is evident that the surface area of the mixed oxides is significantly higher than that of the pure oxides, with a maximum just at the 0·5:0·5 atomic ratio, where the surface area is more than double with respect to the pure oxides. This trend can be related with the lower degree of crystallisation of the mixed oxides with respect to the pure oxides.

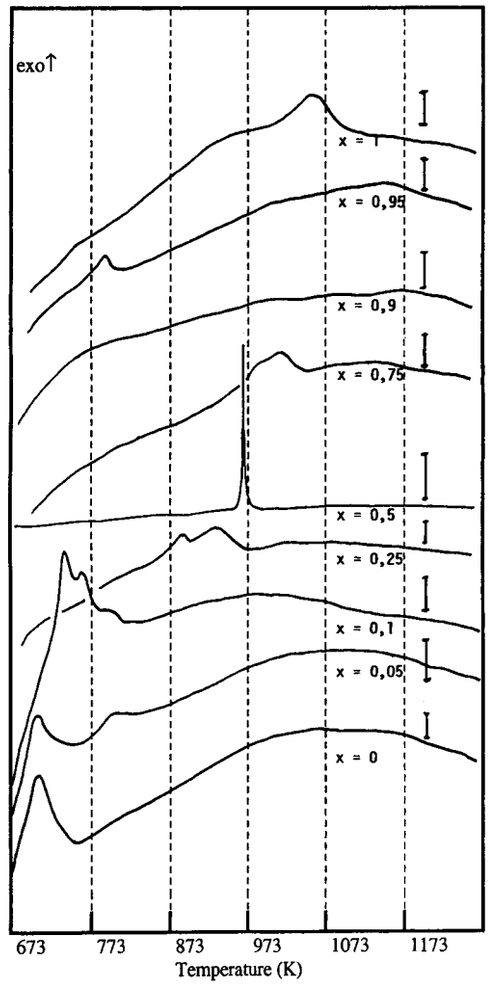

Fig. 1. DTA curves of samples. The bars represent 25 mV DTA signal for all samples except the sample with $x = 0{\cdot}5$, where the bar represents 250 > mV.

3.3 Vibrational spectroscopic characterisation

The IR and Raman spectra of the two main zirconia polymorphs, monoclinic and tetragonal, have been the object of previous studies.[22–26] For monoclinic zirconia (C_{2h}^5 space group, $Z = 4$) the following irreducible representation for the optical modes is valid:

$$\Gamma_{opt} = 9A_g(R) + 9B_g(R) + 8A_u(IR) + 7B_u(IR)$$

which means that 18 Raman active modes and 15 IR active modes are expected. For tetragonal ZrO_2 (space group D_{4h}^{15} with $Z = 2$) instead the following irreducible representation for the optical modes is expected:

$$\Gamma_{opt} = A_{1g}(R) + 2B_{1g}(R) + 3E_g(R) + A_{2u}(IR) + 2E_u(IR)$$

which means that six Raman active modes and three IR active modes are expected. So, the skeletal spectra of the tetragonal polymorphs are expected to be much simpler than those of the monoclinic one.

The Raman pattern of our pure zirconia sample after calcination at 723 K (Fig. 7) is dominated by peaks at 633, 614, 560, 535, 504, 477, 382, 345, 333, 189, 178, 105 cm^{-1} that compare well with those reported for monoclinic zirconia although with some small shifts. An evident peak at 148 cm^{-1} can be taken as an indication of the presence of tetragonal zirconia while the other peaks typical for this phase are either masked by those of the monoclinic phase or weak. Additional peaks at 309 and 270 cm^{-1} can also be due to the tetragonal phase.[25,26]

The addition of TiO_2 up to 10% mol/mol causes the peak at 148 cm^{-1}, assignable to the tetragonal phase, to increase slightly in intensity with respect to those due to the monoclinic phase, while a strong broad peak centred near 310 cm^{-1} grows. This peak is neither typical of ZrO_2 phases nor of

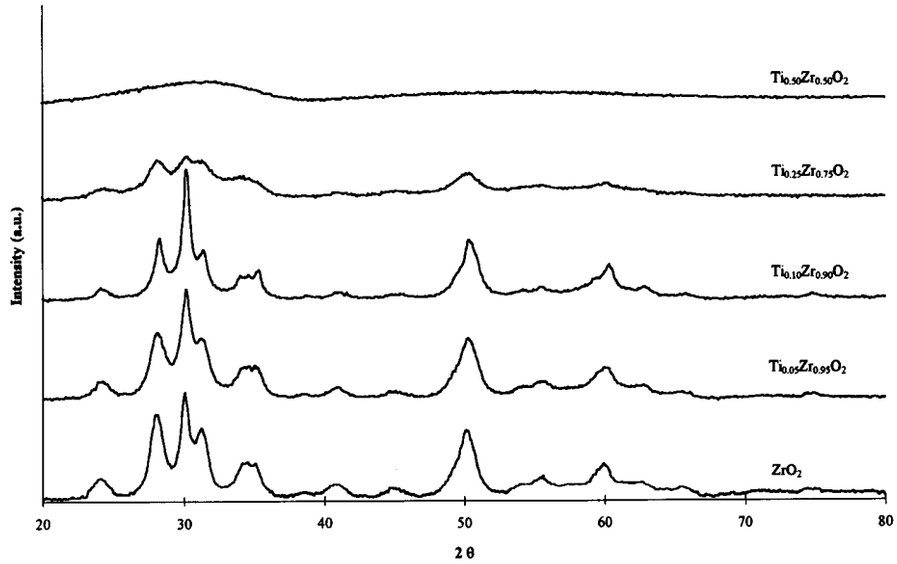

Fig. 2. XRD patterns of the powders with $0 \leq x \leq 0{\cdot}5$ after calcination at 723 K.

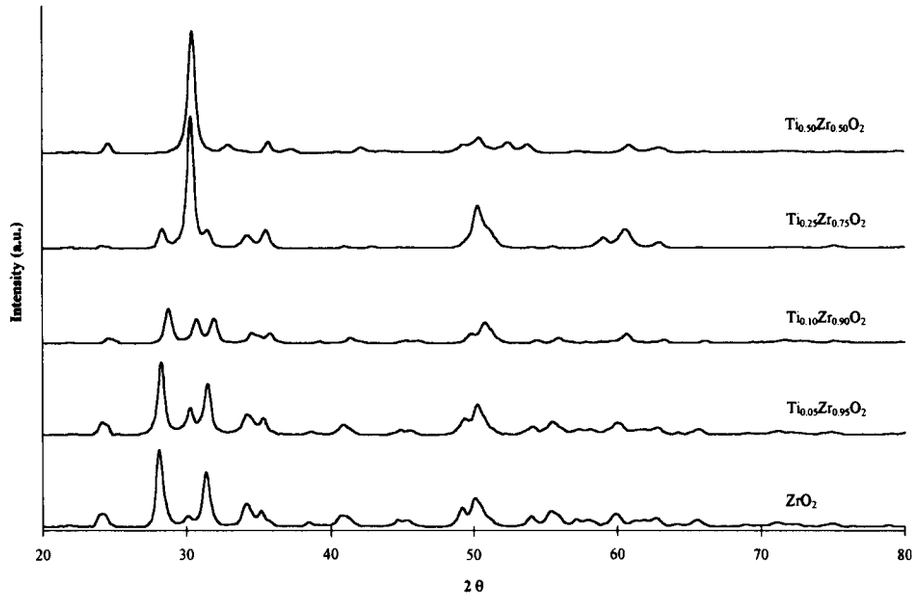

Fig. 3. XRD patterns of the powders with $0 \leq x \leq 0{\cdot}5$ after calcination at 1273 K.

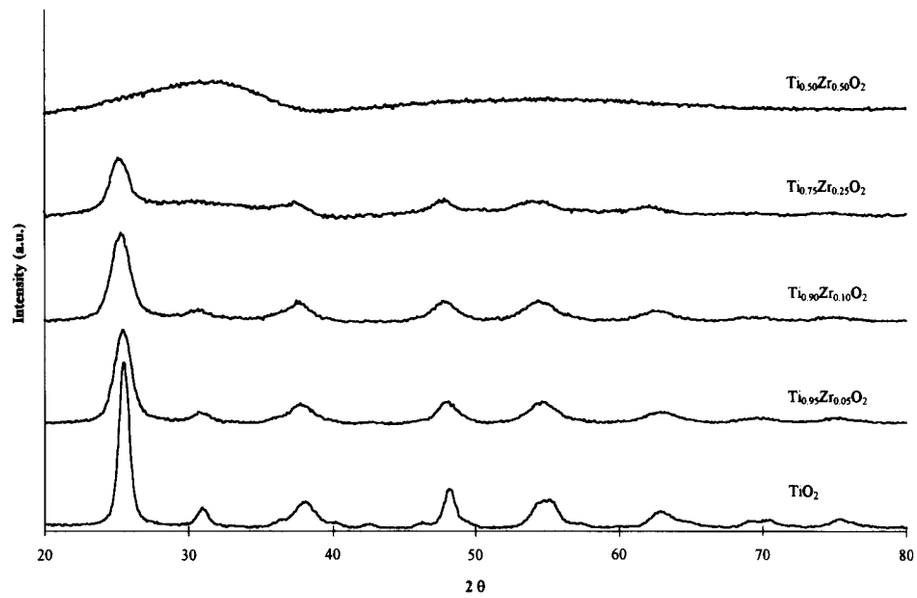

Fig. 4. XRD patterns of the powders with $0{\cdot}75 \leq x \leq 1$ after calcination at 723 K.

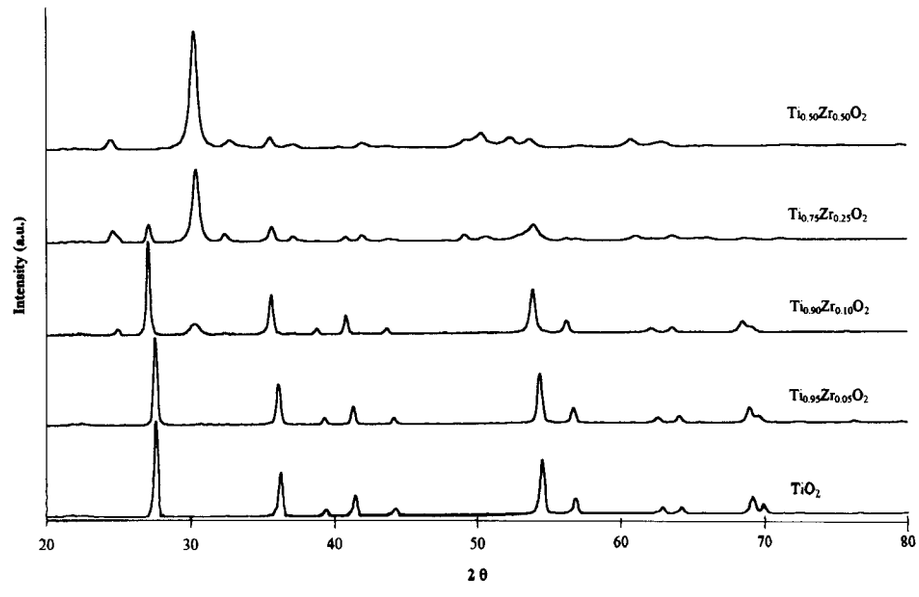

Fig. 5. XRD patterns of the powders with $0{\cdot}75 \leq x \leq 1$ after calcination at 1273 K.

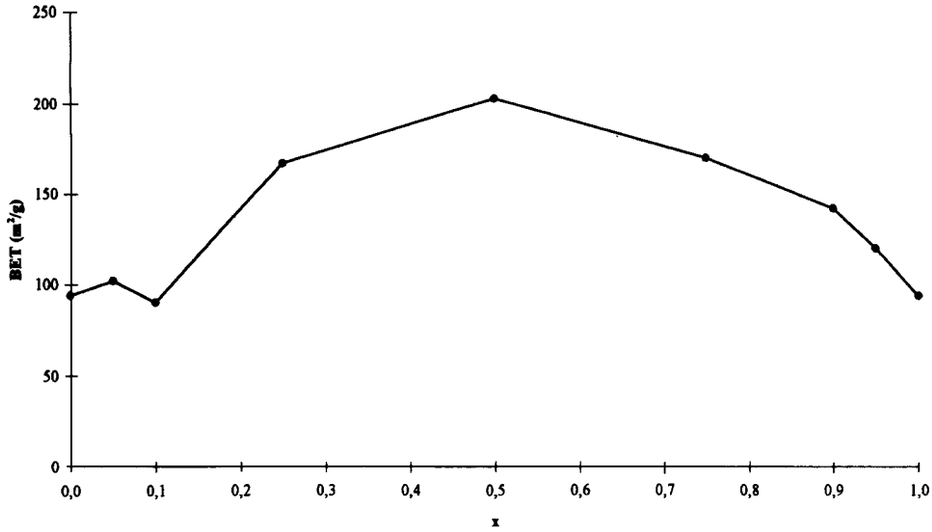

Fig. 6. Surface areas versus composition for the $Zr_{1-x}Ti_xO_2$ samples calcined at 723 K.

TiO_2 phases, and must consequently be assigned to a mixed phase. However, the intensity and relative sharpness of this peak strongly suggests it is due to a crystalline phase. It is in fact well known that Raman peak breadth is quite sensitive to the crystallinity, and that amorphous phases only give rise to extremely broad features, if any. It has however also been found that Raman peaks are very sensitive to ion substitution and that in solid solutions, while IR peaks give rise to shifts, Raman peaks split. So, we can assign the new Raman peak near 310 cm^{-1} to a vibrational mode associated to Ti in solid solution into the ZrO_2 phase(s). This Ti ions lie in an unusually large coordination spheres, here, so that the vibrational frequencies of such Ti–O modes could fall to unusually low frequencies.

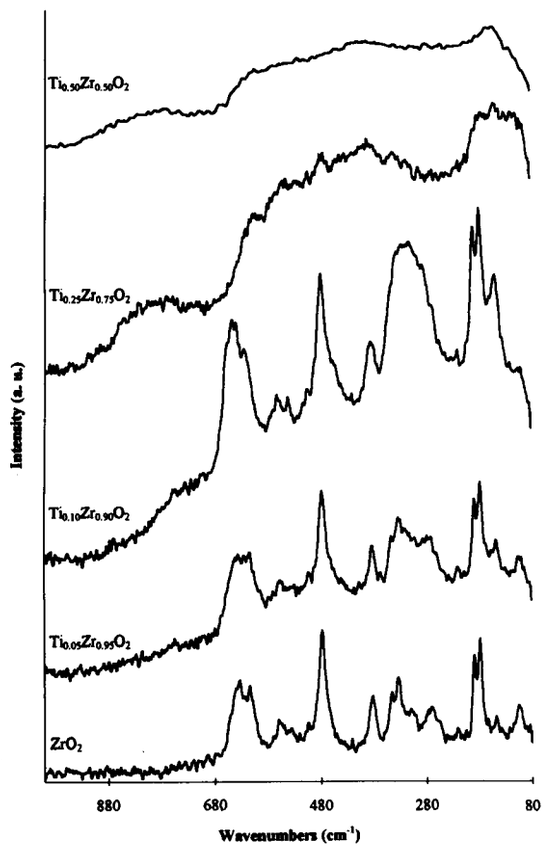

Fig. 7. Ft–Raman spectra of the powders with $0 \leq x \leq 0{\cdot}5$ after calcination at 723 K.

On the other hand, the absolute intensity of the sharp Raman peaks does not decrease upon addition of TiO_2 up to 10% mol/mol (on the contrary, it slightly increases), in agreement with the substantial retention of crystallinity of the zirconia phase observed with XRD, whose peaks are not broadened significantly in this range. However, the sharp peaks are now superimposed on a linebase deviation, probably associated to an increased scattering of the NIR Raman excitation laser beam.

At titanium content higher than 10% the sharp zirconia peaks are lost and only a broad feature is observed, with weak broad peaks at 770, 390 and 152 cm^{-1}.

The IR spectra of the ZrO_2 sample (Fig. 8) shows maxima at 744, 578, 498, 448 and 418, 350, 265, 235 cm^{-1}, with additional components near 665 and 625 cm^{-1}. The spectrum shows the typical features of monoclinic zirconia,[25] although the presence of the tetragonal phase cannot be easily distinguished, because it is responsible only for a broad absorption in the range 700–450 cm^{-1}, according to the literature.[25] In any case, the absolute and the relative intensities of the bands we find in our spectra does not correspond with those reported for 'purely monoclinic' zirconia, so showing that our samples is actually composed by a mixture of the two phases.

The Raman pattern of the TiO_2-rich samples up to the calcination of 723 K up to TiO_2 content of 25% (Fig. 9) show the strongest peaks of anatase near 640, 515, 400 and 143 cm^{-1}, with an additional shoulder near 198 cm^{-1}. These features correspond

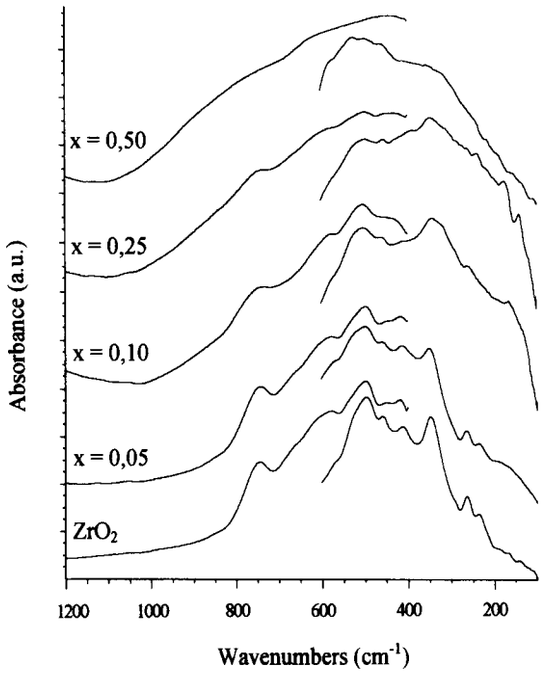

Fig. 8. Ft–IR/Ft–FIR skeletal spectra of the powders with $0 \leq x \leq 0{\cdot}5$ after calcination at 723 K.

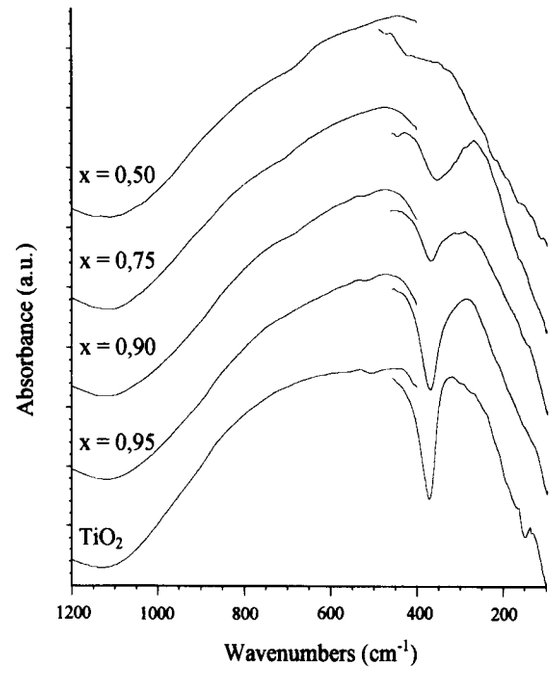

Fig. 10. Ft–IR/Ft–FIR skeletal spectra of the powders with $0{\cdot}75 \leq x \leq 1$ after calcination at 723 K.

to the five Raman active modes of anatase because two of them are actually superimposed near 515 cm^{-1}.[27–29] However, additional small peaks namely at 450, 365, 320, 245 cm^{-1} can also be found, that would correspond to small amounts of brookite,[30] according to the XRD data. Upon Zr addition, small shifts downwards of the main anatase peaks up to 5 cm^{-1} are found and slight peak broadenings, possibly due to a decrease of crystallinity and to the formation of a solid solution. Moreover, the absolute intensity of the anatase pattern progressively decreases of a factor of up to 2·5 for $x = 0{\cdot}75$, and completely disappears for the sample with $x = 0{\cdot}5$. Also in this case a baseline deviation occurs by increasing Zr content.

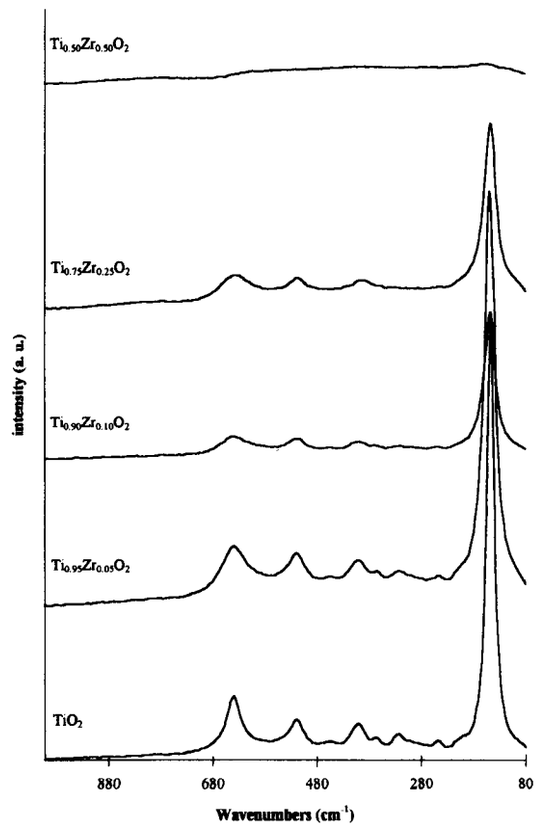

Fig. 9. Ft–Raman spectra of the powders with $0{\cdot}75 \leq x \leq 1$ after calcination at 723 K.

The Ft–IR spectra of the Ti-rich samples (Fig. 10) show the main features due to anatase powder near 450, and 320–285 cm^{-1},[29] and again a progressive broadening and lost of resolution with x increasing up to 0·5.

4 Conclusions

Data on the phase composition of ZrO_2–TiO_2 mixed oxides prepared by coprecipitation are presented here. It has been shown that the addition of titania to the pure zirconia precipitate modifies progressively the crystallisation behaviour of zirconia. In particular titania favours the formation of monoclinic versus tetragonal zirconia, although the main effect is the inhibition of the crystallisation of either ZrO_2 phases. The sample with equimolar amounts of TiO_2 and ZrO_2 looks completely amorphous until near 970 K when Ti zirconate, $ZrTiO_4$, appears by a fast crystallisation process. This apparently occurs in our conditions significantly below the temperature where the $ZrTiO_4$ phase is thermodynamically stable (above 1373 K[20]), i.e. in a range where segregation of $ZrO_2 + ZrTi_2O_6$ is expected.[20] On the other hand,

using our microcrystalline samples we could hardly distinguish by XRD the patterns of $ZrTiO_4$ and of $ZrTi_2O_6$, which are closely related.

The $ZrTiO_4$ phase is likely present also in the samples with $x = 0{\cdot}25$ and possibly 0·1, when calcined at 1273 K. On the other hand, both XRD and Raman spectroscopy show that Ti cations enter in quite a significant amount into the monoclinic zirconia phase, giving rise to Ti–O bonds weaker than those typical for TiO_2.

In the opposite side of the compositional range a similar progressive hindering of the crystallisation of the metastable TiO_2 phase anatase by ZrO_2 is found. On the other hand, ZrO_2 clearly interferes also with the transformation of anatase into rutile, the thermodynamically stable titania polymorph. Crystallisation of $ZrTiO_4$ and the formation of rutile appear to be almost simultaneous processes. The excess of titanium gives rise apparently to a solid solution into $ZrTiO_4$, in agreement with the literature,[20,31] and shifts to higher temperatures the transition giving rise to crystalline $ZrTiO_4$.

The mutual hindering of crystallisation can be related with the quite limited mutual miscibility of the two pure oxides in their own structures.[29] In fact Zr^{4+} ion is definitely larger (0·79 Å in ZrO_2) than Ti^{4+} ion (0·60 Å). This also affects the preferred coordination of Zr^{4+} in oxides (seven to eight) larger than that of Ti^{4+} (always six). Interestingly, however, Zr^{4+} and Ti^{4+} are randomly distributed in the octahedral-like PbO_2-type structure of $ZrTiO_4$. On the other hand, this phase is unstable at low temperature when the component oxides or PbO_2-type structures with ordered cation distribution tend to form.[20] This means that titanium and zirconium ions can easily exchange each other only at temperatures at which solid-state diffusion can occur. Both TiO_2 ($T_f = 2109$ K) and ZrO_2 ($T_f = 2970$ K) and $ZrTiO_4$ as well (incongruent fusion at $T_f = 2090$ K) are quite refractory materials. The temperature at which solid state diffusion becomes significant is expected to be relatively high. According to Tamman[32] this temperature can be estimated to be in the range 1100 K ÷ 1576 K for ZrO_2 and in the range 850 K ÷ 1118 K for both TiO_2 and $ZrTiO_4$. In fact, we observe the crystallisation of $ZrTiO_4$ just in the last range, 970 K.

The stabilisation of the amorphous state for compositions near those of $ZrTiO_4$ (i.e. equimolari TiO_2–ZrO_2) and, to a lesser extent also for the other compositions in the $Zr_{1-x}Ti_xO_2$, if calcination temperature below the above ranges of solid state diffusion, allows to obtain very dispersed high surface area materials.

According to the relevance of amorphous high area powders in heterogeneous catalysis and to the possibility to make them microporous by adding, upon preparation, appropriate templating agents,[33] the 1:1 ZrO_2–TiO_2 powders below the crystallisation temperature of $ZrTiO_4$ are of interest. The application of this composition for supporting metal oxide catalysts is now under study.

References

1. Buchner, W., Schliebs, G., Winter G. and Buchel, K. H., *Industrial Inorganic Chemistry*. VCH, Berlin, 1989.
2. Wainwright, M. S. and Foster, N. R., Catalysts, kinetics and reactor design in phthalic anhydride synthesis. *Catal. Rev. Sci. Eng.*, 1979, **19**, 211.
3. Nikolov, V. A. and Anastasov, A., Pretreatment of a vanadia–titania catalyst for partial oxidation of o-xylene under industrial conditions. *Ind. Eng. Chem. Res.*, 1992, **31**, 80–88.
4. Cho, S. M. *Chem. Eng. Progr* 1994 **90**(I), 39.
5. Forzatti, P. and Lietti, L., Recent advances in de-NO_xing catalysis for stationary applications. *Heter. Chem. Rev.*, 1996, **3**, 33.
6. Ramirez, J., Ruiz-Ramirez, L., Cedeno, L., Harle, V., Vrinat, M. and Breysse, M., *Appl. Catal. A. General*, 1993, **93** 163.
7. Topsøe, H., Clausen, B. S., and Massoth, F. E., in *Catalysis Science and Technology*, Vol. 11, ed. J. R. Anderson and M. Boudart. Springer Verlag, Berlin, 1996, p. 1.
8. Hébrard, J. L., Nortier, P., Pijolat, M. and Soustelle, M., *J. Amer. Ceram. Soc.*, 1990, **73**, 79; Hébrard, J. L., Dauzat, M., Pijolat, M. and Soustelle, M., *C. R. Acad. Sci. Paris*, Ser II, 1987, **305**, 1185.
9. Oliveri, G., Ramis, G., Busca, G. and Sanchez Escribano, V., *J. Mater. Chem.*, 1993, **3**, 1239–1249.
10. Barin, I., *Thermochemical Data of Pure Substances*. Verlag Chemie, Berlin, 1989.
11. Cristiani, C., Bellotto, M., Forzatti, P. and Bregani, F., *J. Mater. Res.*, 1993, **8**, 2019.
12. Gallardo Amores, J. M., Sanchez Escribano, V. and Busca, G., *J. Mater. Chem.*, 1995, **5**, 1245.
13. Maugé, F., Duchet, J. C., Lavalley, J. C., Houssenbay, S., Payen, E. and Gromblot, J., *Catal. Today*, 1991, **10**, 561.
14. Szakacs, S., Altena, G. J., Fransen, T., van Ommen, J. G. and Ross, J. R. H., *Catal. Today*, 1993, **16**, 237.
15. Subba Rao, E. C., Maiti, H. S. and Srivastava, K. K., *Phys. Status Solidi*, 1974, **A21**, 9.
16. Barker, W. W., Bailey, F. P. and Garrett, W., *J. Solid State Chem.*, 1973, **7**, 448.
17. Moulson, A. J. and Herbert, J. M., *Electroceramics*. Chapman and Hall, London, 1990, p. 239.
18. Negas, T., Yeager, G., Bell, S. and Amren, R., in *Chemistry of Electronic Ceramic Materials*, ed. K. Davies and R. S. Roth. Nat. Inst. Standard and Tech., Washington, DC 1990, p. 21.
19. West, A. R., *Solid State Chemistry and its Applications*. Wiley, New York, 1984.
20. McHale, A. E. and Roth, R. S., *J. Am. Ceram. Soc.*, 1986, **69**, 827.
21. Hirata, T., Kitajima, M., Nakamura, K. G. and Asaris, E., *J. Phys. Chem. Solids*, 1994, **55**, 349.
22. Hirata, T., Zhu, H., Furubayashi, T. and Nakatani, I., *J. Am. Ceram. Soc.*, 1993, **76**, 1361.
23. Perry, C. H., Liu, D. W. and Ingel, R. P., *J. Am. Ceram. Soc.*, 1985, **68**, C184.
24. Kim, D. J., Jung, H. J. and Yang, I. S., *J. Am. Ceram. Soc.*, 1993, **76**, 2106.
25. Hirata, T., Aasari, E. and Katajima, M., *J. Solid State Chem.*, 1994, **110**, 201.
26. Kim, B. K., Hahn, J. W. and Han, K. R., *J. Mat. Sci. Lett.*, 1997, **16**, 669.

27. Ohsaka, T., Izumi, F. and Fujiki, Y., *J. Raman Spectrosc.*, 1978, **7**, 321.
28. Balachandran, U. and Eror, N. G., *J. Solid State Chem.*, 1982, **42**, 276.
29. Busca, G., Ramis, G., Gallardo Amores, J. M., Sanchez Escribano, V. and Piaggio, P., *J. Chem. Soc. Faraday Trans.*, 1994, **90**, 3181.
30. Arkipenkpo, D. K., Bobovich, Ya. S. and Tsenter, M. Ya., *Zh. Prikl. Spectrosc.*, 1984, **41**, 1984.
31. Yamaguchi, O. and Mogi, H., *J. Am. Ceram. Soc.*, 1989, **72**, 1065.
32. Davidson, A. and Che, M., *J. Phys. Chem.*, 1992, **96**, 9909.
33. Beck, J. S., Vartuli, J. C., Roth, W. J., Leonowicz, M. E., Kresge, C. T., Scmitt, K. D., Chu, C. T. W., Olson, D. H., Sheppard, E., McCullen, S. B., Higgins, J. B. and Schlenker, J. L., *J. Am. Chem. Soc.*, 1992, **114**, 10834.